A new insight into design of acoustic liner arrays arrangement in the presence of a grazing flow

Hadi Dastourani and Iman Bahman-Jahromi*

Department of Aeronautical Science & Technology, Khayyam Research Institute, 14665-834, Tehran, Iran

Abstract.   This study evaluated the acoustic performance of two configurations of serial HR arrays and lined HR arrays in the presence of grazing flow using a 3D numerical simulation. The dual, triple, and quad HR arrays were compared to the conventional HR array. The simulation results showed that the number of resonant frequencies increased with the number of serial HR arrays. The C_{TL} did not significantly change with the number of serial HR arrays. The acoustic performance of the two, three, and four-lined HR arrays was compared to the conventional HR array. The results showed that the resonant frequency and TLmax increased with the number of lined HR arrays. The C_{TL} also increased with the number of lined HR arrays. The effect of the grazing flow Mach number (M_a) was investigated on the four-lined HR array configuration and compared to the conventional HR configuration. TLmax and C_{TL} decreased for both configurations with increasing M_a. The four-lined HR array configuration had significantly better acoustic performance than the conventional HR configuration. The TLmax and CTL increased by more than 300% when the configuration was changed from the conventional HR to the four-lined HR array at M_a = 0. The increment percentage decreased with increasing M_a.

1. Introduction

The development of technology and the increasing use of machinery have both advantages and disadvantages. One of the disadvantages is noise pollution, which is becoming more of a problem as technology advances. Various methods are used to reduce noise. The most efficient way is the reduction of noise generation by machinery by applying new manufacturing technologies to control noise at the sources. Furthermore, sound-absorbing materials and acoustic liners are widely used to suppress and reduce the noise emission from air-conditioning systems, ducts, and aircraft engines (Qiu *et al.* 2018, 2019, Wang and Zhang 2013).

Aircraft noise is the second most annoying noise after road traffic noise, especially in areas around airports. The International Civil Aviation Organization (ICAO) first introduced aircraft noise regulations for noise control near airports in the late 1960s (Žilienė and Stankūnas 2002, Ma and Su 2020). The main source of noise in aircraft is the turbofan engine. The turbofan engine noise propagates out of the engine through the inlet and outlet of the engine. Acoustic liners are

---

*Corresponding author, Assistant Professor, E-mail: bahman@ari.ac.ir

[a] Ph.D., E-mail: hadi.dast@gmail.com
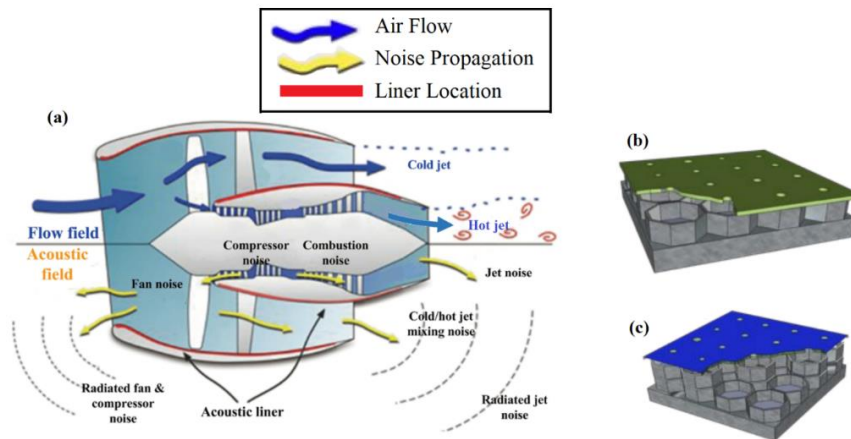
Fig. 1 (a) Noise radiation pattern of the aircraft engine, (b) SDOF, and (c) DDOF acoustic liner (Bertolucci 2012)
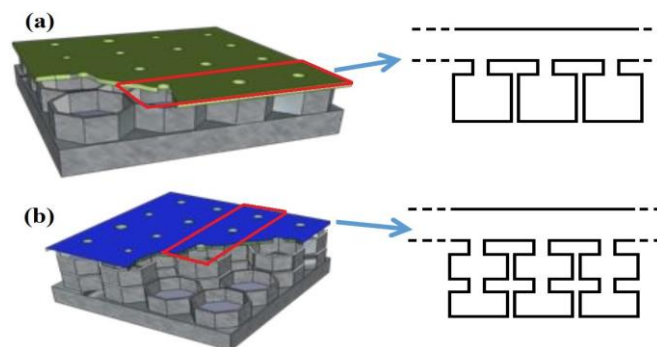
Fig. 2 The similarity between (a) SDOF liner and an array of single HRs (b) DDOF liner and array of dual HRs

placed on the internal wall of the nacelle to reduce the turbofan noise, as shown in Fig. 1 (a) (Bertolucci 2012). These liners are designed to attenuate noise at frequencies that are effective in environmental noise pollution. There are two general types of acoustic liners used in turbofan engines, including single-degree freedom (SDOF) and double-degree freedom (DDOF) liners (Sugimoto *et al*. 2012, Jing *et al*. 2023, Zhao 2011).

An SDOF acoustic liner consists of a perforated sheet supported by a single layer of honeycomb cells and a rigid backing plate (Fig. 1b). A DDOF liner has two layers of honeycomb cells separated by another perforated sheet (Fig. 1c). In the conventional SDOF acoustic liner, the honeycomb cavity has impenetrable walls. Therefore, the sound waves cannot move parallel with the perforated face sheet (Ma and Su 2020). Hence, an SDOF acoustic liner is equivalent to an array of single HRs and a DDOF acoustic liner is equal to an array of dual HRs (Fig. 2).

Helmholtz resonators (HRs) are a basic element in acoustic liner design. Advanced HR design is essential for pipe noise abatement and combustion instability control (Zhang *et al*. 2015, 2021). According to aforementioned applications, increasing the acoustic performance of HRs has attracted large attention in later researches (Meissner 2002, Langfeldt *et al*. 2020, Zhao *et al*. 2017, Mahesh *et al*. 2021). In the current study, the acoustic characteristics of different configurations of

the HR arrays are evaluated. Before that, a brief overview of the research done in this area is provided. Ingard (1953) investigated the impact of the neck geometry and Chanaud (1994) studied the effect of the orifice section shape such as circular, rectangular and cross-shaped on the resonance frequency of an HR.

Selamet and co-workers studied the effect of the resonator cavity volume, and the height to diameter ratio of the cylindrical resonator. In this regard, they developed a three-dimensional boundary element method and one, two, and three-dimensional analytical models (Dickey and Selamat 1996, Selamat *et al*. 1997, Selamat and Ji 2000). The neck length affects the resonant frequency of an HR. the extended neck is a way to increase neck length. Selamet and Lee (2003) and Bi *et al*. (2012) appraised the effect of an extended neck on the HR acoustic performance. Zhao (2012) and Zhao *et al*. (2022) investigated shape effect of coupled HR with two resonators connected via a thin compliant membrane.

Numerical simulations are largely used in computational design (Igali *et al*. 2020, Rode *et al*. 2021). Selamet *et al*. (2011) used STAR-CD software and Lu *et al*. (2019) used COMSOL Multiphysics to investigate the effect of the neck offset on the acoustic performance of an HR in the presence of a grazing flow. Wu *et al*. (2019) evaluated the effects of the grazing flow and the dimensions of neck on the aeroacoustics damping performance of a Helmholtz resonator numerically.

They applied 2D numerical simulations by COMSOL Multiphysics software.

To improve the transmission loss performance of an HR, Guan *et al*. (2020) proposed a modified design of an HR by implementing a rigid baffle in its cavity. They evaluated the effects of the rigid baffle width, location, implementation configurations (i.e. attached to the right sidewall or left sidewall), and neck shape. They also considered the grazing flow Mach number and used COMSOL Multiphysics for simulations. Mahesh and Mini (2021) studied the normal incidence sound absorption characteristics of series and parallel configurations of Helmholtz resonators and showed that the analytical model matches with the FEM results of COMSOL Multiphysics simulations.

In the present study, the effects of different configuration arrangements, including the serial HR array and the lined HR array, are studied in the presence of a grazing flow. In this regard, a 3D numerical approach based on the COMSOL Multiphysics software has been applied. In section 2, the numerical solution approach and the validation test are explained. The third section of this paper presents the simulation results for different configuration arrangements of the HRs array. Finally, the article closes in section 4 with a summary and some conclusions.

2. Solution approach and validation studies

The mesh dependency and validation tests are important considerations in the numerical simulation of fluid flows. A brief overview of these tests is presented in this section, and a more detailed discussion can be found in our previous paper (Dastourani and Bahman-Jahromi 2021).

2.1 Equations and solution approach

In this work, the acoustic performance of the Helmholtz resonators system with different configuration arrangements, including the serial HR array (Fig. 3a) and the lined HR array (Fig. 3, b), is investigated. In this regard, the numerical method has been used. Two physics, "single-
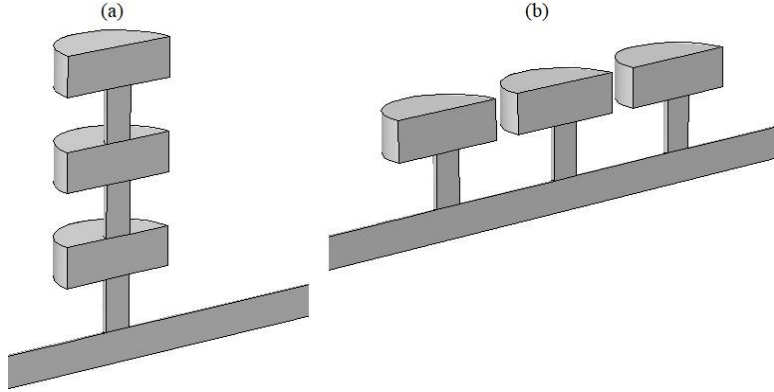
Fig. 3 (a) Serial Helmholtz resonator array configuration, (b) lined Helmholtz resonator array configuration

phase fluid flow" and "acoustic waves" are involved in this problem. In the current work, COMSOL Multiphysics software is used and the simulations are performed in a three-dimensional state. The single-phase airflow inside the duct and the Helmholtz resonator configurations are defined as a grazing flow with a Mach number Ma. Ma in the current work varies between 0 to 0.40. Therefore, the Reynolds number for $Ma > 0.003$ is greater than 3200 and the flow is turbulent. Here, for the simulation of the turbulent flow field in the Helmholtz resonator system, the Turbulent Flow k-ε interface from the CFD module of COMSOL Multiphysics software has been used (COMSOL AB, 2020).

The Linearized Navier-Stokes equations are used to simulate the acoustic field. In this case, the equations of continuity, momentum and energy in the frequency domain are as follows,

$$i\omega\rho_t + \nabla \cdot (\rho_t \vec{u}_0 + \rho_0 \vec{u}_t) = M \tag{1}$$

$$\rho_0(i\omega\vec{u}_t + (\vec{u}_t \cdot \nabla)\vec{u}_0 + (\vec{u}_0 \cdot \nabla)\vec{u}_t) + \rho_t(\vec{u}_0 \cdot \nabla)\vec{u}_0 = \nabla.\sigma + \vec{F} - \vec{u}_0 M \tag{2}$$

$$\rho_0 C_p(i\omega T_t + \vec{u}_t \cdot \nabla T_0 + \vec{u}_0 \cdot \nabla T_t) + \rho_t C_p(\vec{u}_0 \cdot \nabla T_0) - \alpha_p T_0(i\omega p_t + \vec{u}_t \cdot \nabla p_0 + \vec{u}_0 \cdot \nabla p_t) \\ - \alpha_p T_t(\vec{u}_0 \cdot \nabla p_0) = \nabla.(k\nabla T_t) + \Phi + Q \tag{3}$$

where $\vec{u}$, p and T are the velocity, the pressure, and the temperature, respectively. In addition, the variables with zero subscripts are the background mean flow values. Also, the subscript "t" represents the total acoustic field variables, that is, the sum of the scattered fields and the background acoustic fields as follows,

$$p_t = p + p_b, \qquad \vec{u}_t = \vec{u} + \vec{u}_b, \qquad T_t = T + T_b \tag{4}$$

where the subscript "b" refers to the background acoustic field. In the Eqs. (1) to (3) M, Q and $\vec{F}$ are the source terms. Also σ, Φ, and ρ_t are the stress tensor, the viscous dissipation, and the density, respectively. They are presented as,

$$\sigma = -p_t I + \mu(\nabla\vec{u}_t + (\nabla\vec{u}_t)^T) + (\mu_B - \frac{2}{3}\mu)(\nabla \cdot \vec{u}_t)I \tag{5}$$

where μ is the dynamic viscosity, μ_B is the volume viscosity, I is the identity tensor, τ_{ij} is the
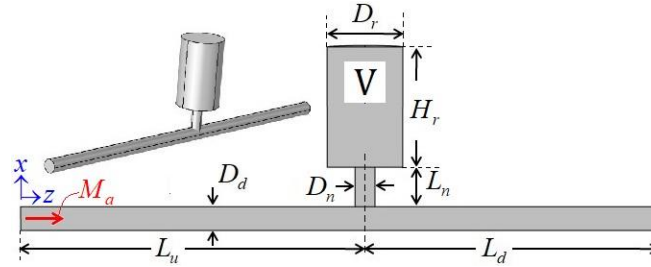
Fig. 4 A schematic of the Helmholtz resonator

Table 1 The geometry dimensions and the flow conditions for the conventional HR

Parameter	Value	Parameter	Value
L_u (cm)	70	M_a	0 - 0.10
L_d (cm)	60	f (Hz)	10 - 300
L_n (cm)	8.05	c_0 (ms^{-1})	343
D_r (cm)	15.32	ρ_0 (kgm^{-3})	1.2
D_d (cm)	4.86	p_0 (atm)	1.0
D_n (cm)	4.044	T_0 (^{0}C)	25
H_r (cm)	24.42	μ_{air} (μPa.s)	18.5

$$\Phi = \tau_{ij} \frac{\partial u_i}{\partial x_j} . \tau_{ij} \tag{6}$$

$$\rho_t = \rho_0 (\beta_T p_t - \alpha_p T_t) \tag{7}$$

viscous stress tensor, β_T is the isothermal compressibility, and α_p is the thermal expansion coefficient. The Linearized Navier-Stokes (LNS), Frequency Domain interface from the Acoustics module COMSOL Multiphysics software is applied here for modeling the acoustic field (COMSOL AB, 2020).

The geometry of the duct with a conventional HR is shown in Fig. 4 and its dimensions are shown in Table 1. As mentioned before, two physics of the CFD and Acoustics are involved in the present simulation. For the simulation of CFD, a very fine and as much as possible, structured mesh is required. For modeling acoustics, a coarser mesh rather than CFD and non-structure is better suited. Accordingly, two different meshes are considered to solve the flow and the acoustics fields, as shown in Fig. 5 for a conventional HR. After the Mesh independence investigation, the mesh with 1192483 elements was chosen for the CFD field and the mesh with 128330 elements was chosen for the acoustics field. The mesh dependency is discussed in section 2.2.

The solution approach is: at first, in the mesh of Fig. 5(a) the equations of single-phase airflow with the k-ε turbulence model are solved by considering the velocity as input, based on the Mach number studied in the current study, then applying the mapping method and Solving PDE Equations (the Weak Form PDE interface from the Mathematics module), output parameters including pressure, velocity and turbulent viscosity are mapped from the flow field mesh (Fig. 5a) onto acoustic field mesh (Fig. 5b). Next, for the acoustic field, the linearized Navier-Stokes
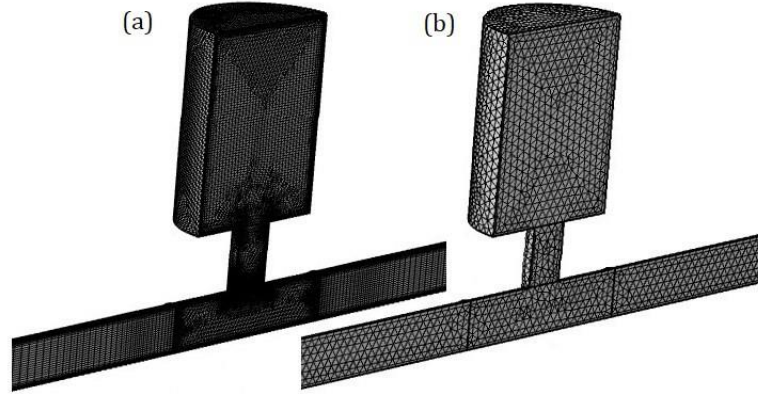
Fig. 5 A schematic of mesh for (a) the flow field solution (b) the acoustic field solution

equations are solved in the frequency domain by applying the background flow parameters from the flow field solution and the plane wave from the noise source as the input data. The Perfectly Matched Layer (PML) boundary domain is used at both ends of the duct as a non-reflecting boundary condition. The plane wave variables are defined according to,

$$p_b = p_i e^{-ikz}, \qquad k = \omega/(C_{0+}U_{in}) \tag{8}$$

$$\vec{u}_b = (0,0, -\frac{1}{i\omega\rho_0}\frac{\partial p_b}{\partial z}) \tag{9}$$

$$T_b = \frac{\alpha_p T_0}{\rho_0 C_p} p_b \tag{10}$$

where pi is incident the acoustic wave amplitude, $k0$ is the wavenumber, ω is the angular frequency, $c0$ is the sound speed of air, Uin is the input velocity ($Uin = Mac0$, Ma is Mach number of airflow), $\rho0$ is the air density, and Cp is the heat capacity at the constant pressure. After solving the acoustics field, the transmission loss (TL) is calculated as,

$$\text{TL} = 20log_{10}(\left|\frac{p_i}{p_{out}}\right|) \tag{11}$$

where Pout represents the transmitted acoustic wave on the upstream duct.

2.2 Mesh dependency

As mentioned before, in the work, two different meshes are used to solve the CFD field and the Acoustics field. For a conventional HR (Fig. 4), the solution independence of the CFD field from the mesh size is done. In this regard, three meshes with the domain elements of 623912 ($D_n/\Delta z = 22$), 1192483 ($D_n/\Delta z = 34$) and 1631428 ($D_n/\Delta z = 41$) are considered in the HR system. Fig. 6 shows the velocity profile in the neck inlet for $M_a = 0.1$. According to this figure, the mesh with 1192483 elements and $D_n/\Delta z = 34$ was choose for the CFD field. The same work is accomplished for the acoustics field. The simulations were performed in chosen mesh of the CFD field, $M_a = 0.1$ and three meshes with 65016, 128330 and 345378 domain elements for acoustics field. According to Fig. 7, the mesh with 128330 elements was choose for the acoustics field.
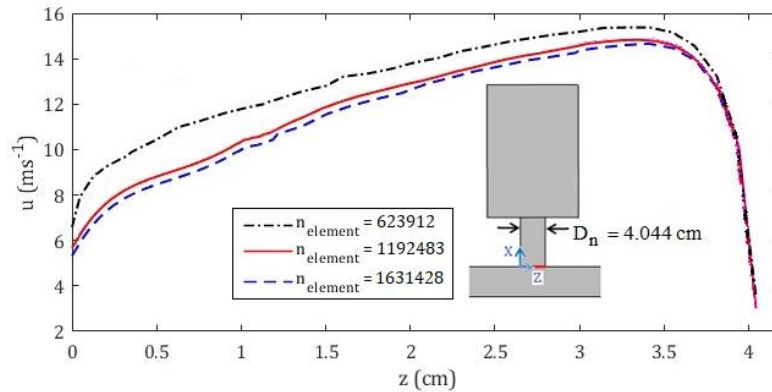
Fig. 6 Velocity profile in the neck inlet for the various mesh size of the CFD field
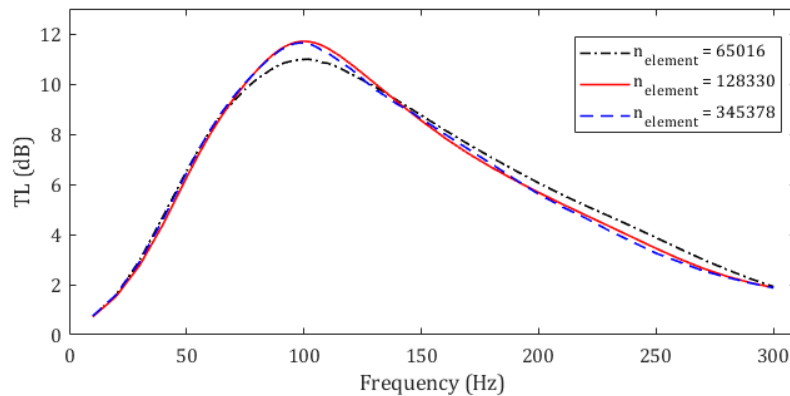
Fig. 7 Transmission loss for the various mesh size of the acoustics field

2.3 Verification study

To determine the accuracy of the numerical approach, as well as the correctness of the achieved results, the simulations are performed for a conventional HR geometry and flow conditions according to the experimental work of Selamet *et al*. (Selamat *et al*. 2011). The dimensions of the HR system and flow conditions have been shown in Table 1. Fig. 6 depicts the TL versus the frequency for the results obtained in the current study as compared with the experimental work of Selamet *et al*. (2011). As can be seen, the present numerical results are in good agreement with the experimental data, which proves the validity of the results in addition to the appropriateness of the simulation approach utilized in this study.

3. Results and discussion

In the present study, the transmission loss performance of the HR arrays has been investigated in the presence of the grazing flow. In this regard, the configuration effects of the serial HRs array and lined HR array have been evaluated at various flow Mach numbers.
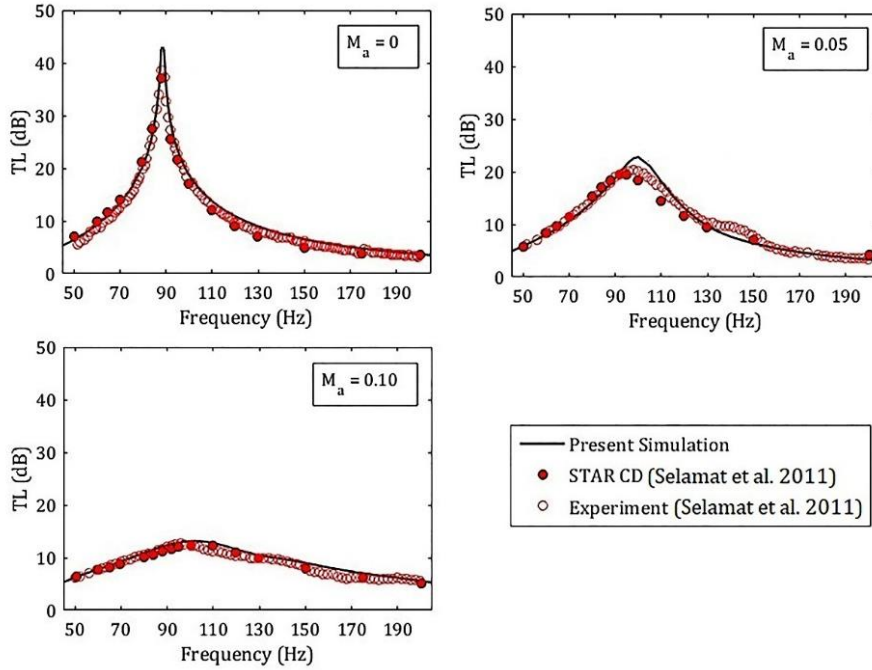
Fig. 8 Transmission loss against frequency, comparison between the simulation and the experiment (Selamet *et al.* 2011)
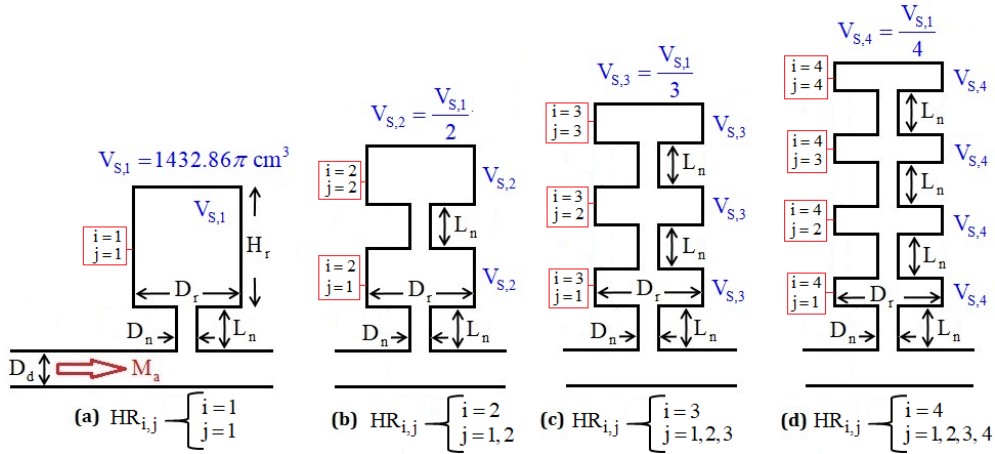
Fig. 9 A schematic of serial HR array (a) single (or conventional) (b) dual (c) triple and (d) quad HR array

3.1 A serial Helmholtz resonator array

A serial HR array is formed by several (more than one) HRs connected in series, as shown in Fig. 9. Applying two HRs, i.e., neck-cavity-neck-cavity, (Fig. 9b) is known as the dual HR system. A dual HR could be equivalent to a part of a DDOF acoustic liner. In this section, the acoustic performance of single, dual, triple, and quad HR arrays will be evaluated in the presence of the

Table 2 Flow conditions and geometric dimensions of the serial HR array

Parameter	Value	Parameter	Value
L_u (cm)	70	$V_{S,1}$ (cm^3)	1432.86π
L_d (cm)	80	$V_{S,2}$ (cm^3)	716.43π
L_n (cm)	8.05	$V_{S,3}$ (cm^3)	477.62π
D_d (cm)	4.859	$V_{S,4}$ (cm^3)	358.22π
D_n (cm)	4.044	M_a	0 – 0.10
D_r (cm)	17.7	f (Hz)	5 - 500
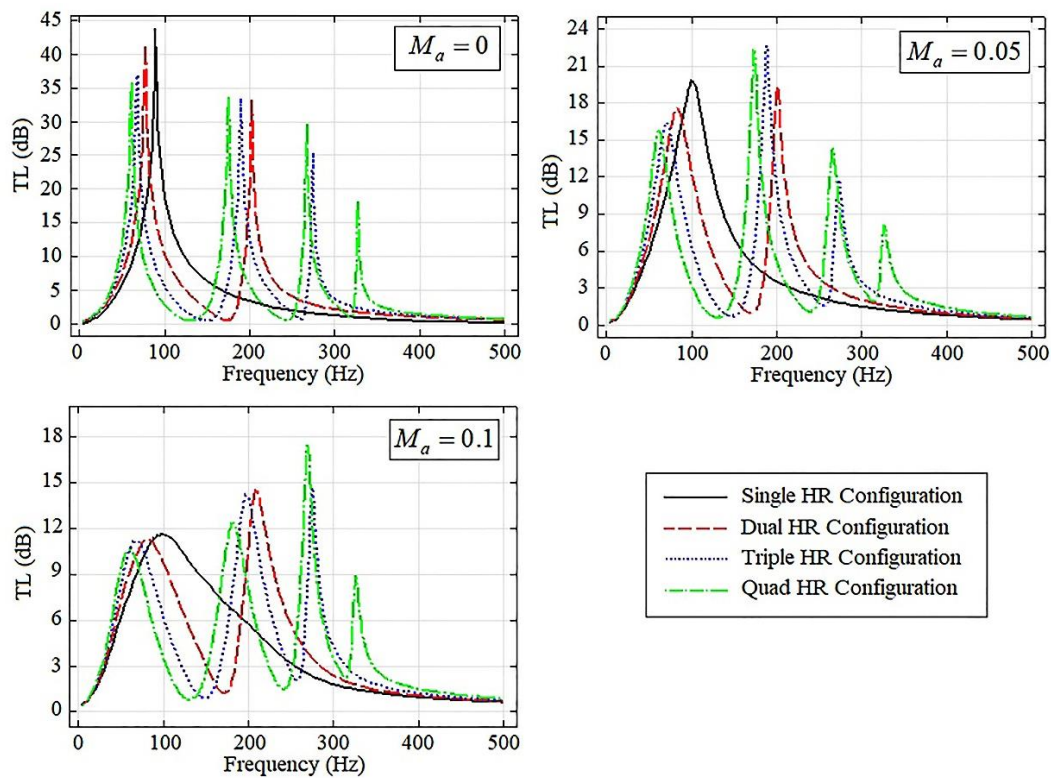
Fig. 10 Transmission loss versus frequency for the different serial HR array configurations in various Mach numbers

grazing flow. Here, the resonator cavity volume for all configurations (Fig. 9) is equal to each other, so $VS,1 = 2VS,2 = 3VS,3 = 4VS,4 = 1432.86\pi$ $cm3$. The dimensions of HR configurations and the other required parameters are presented in Table 2. In the section, the simulations are performed for various HR configurations according to Fig. 9 in the grazing flow Mach numbers of 0, 0.05, and 0.10. In the figure, i represent to Configuration type (single, dual, triple, and quad HR array), j represent to array number in serial HR array.

Fig. 10 depicts the TL against frequency for four configurations of conventional (single), dual, triple, and quad HR array (Fig. 9) in three Mach numbers, Ma, of 0.0, 0.0,5 and 0.1. It can be seen in the figure, that for the single HR, one resonant frequency is generated. While for the dual HR,
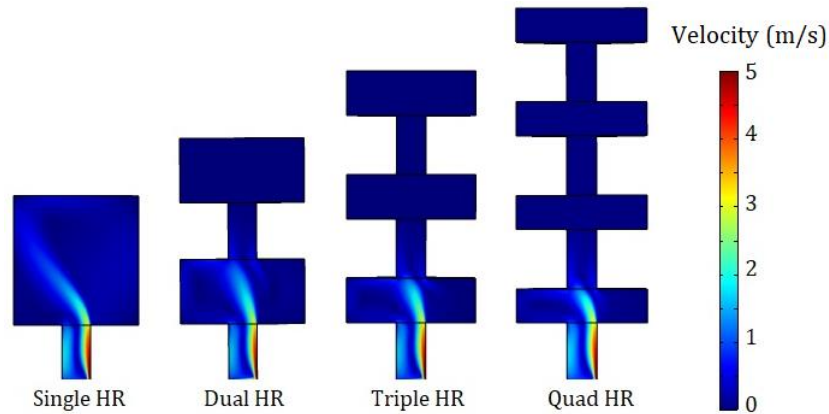
Fig. 11 Velocity contour (Steady State) for the different serial HR array configurations i M_a = 0.05 (Steady State)
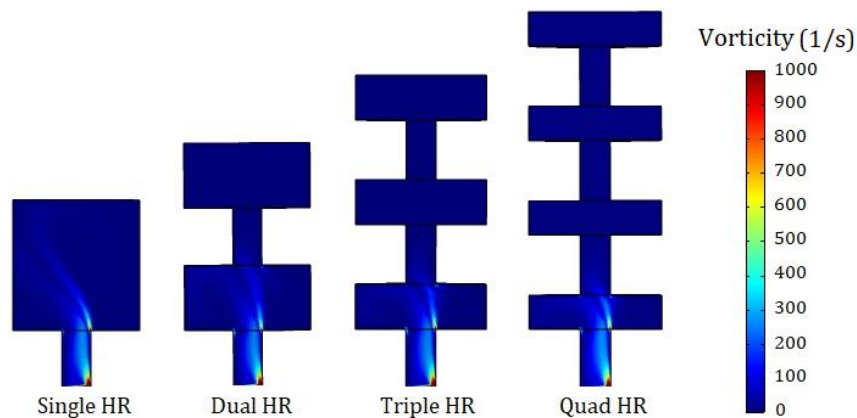
Fig. 12 Vorticity contour (Steady State) for the different serial HR array configurations in M_a=0.05

two resonant frequencies are generated. In other words, with increasing the number of HR arrays the number of resonant frequencies increase so that for any configuration, the number of resonant frequencies is equal to the number of HR arrays. The change of configuration, lead to the changes in the fluid flow pattern in the HRs. As an example, Figs. 11 and 12 depict the velocity, vorticity for the various configurations in M_a =0.05 respectively. The Changes of the flow pattern affect the vortex-sound interaction in the HR. In Figs. 13 and 14 the total acoustic pressure (P_t) and sound pressure level (SPL) have been present for the various configurations in M_a =0.05 respectively. It can be seen in the figures, P_t and SPL change with changing configuration.

Fig. 15, corresponding to Fig. 10, shows the quantitative value of the resonant frequencies for the different configurations for the various M_a. In this figure, i represent to Configuration type (single, dual, triple, and quad HR array), j represent to array number in serial HR array (Fig. 9) and symbols of □, ○ and △ represent to Mach number of 0, 0.05 and 0.1 respectively. As can be seen in Fig. 15, in comparison to the configuration type effect, the Mach number has no significant effect on the resonant frequency, while increasing the Mach number the maximum transmission loss, TL$_{max}$, decreases. In addition, the resonant frequencies decrease with increasing the number
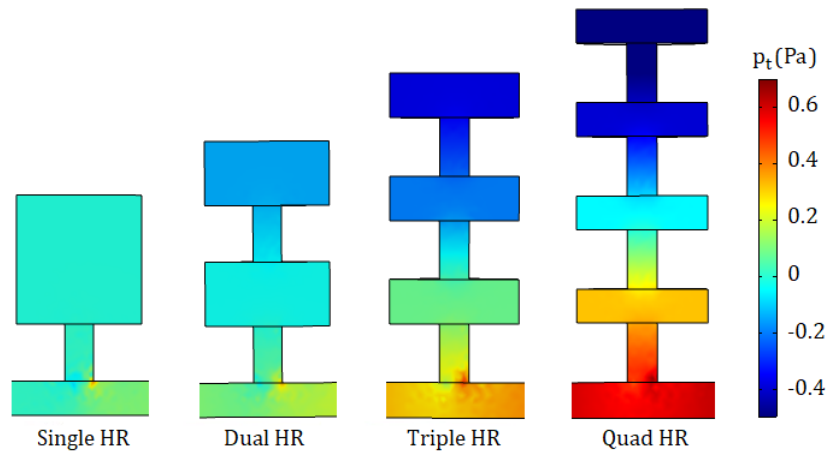
Fig. 13 Total acoustic pressure (Frequency-Domain at 100 Hz) for the different serial HR array configurations in M_a=0.05
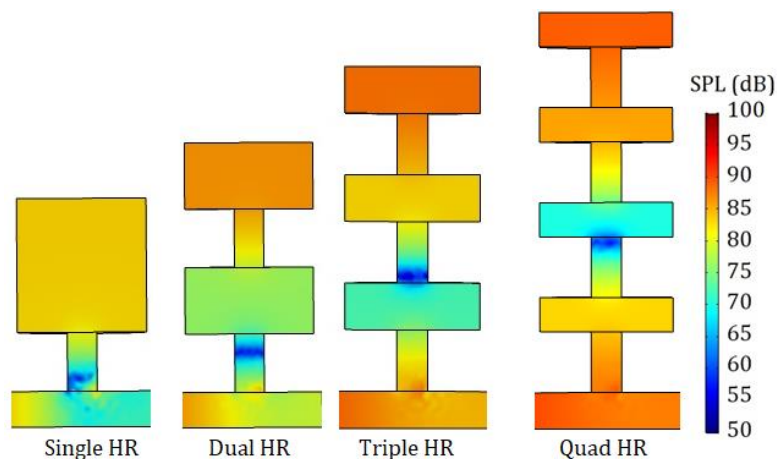
Fig. 14 Sound pressure level (Frequency-Domain at 100 Hz) for the different serial HR array configurations in M_a=0.05

of HR arrays. In contrast, the TL_{max} has a different treatment so that with increasing the number of HR arrays in the Mach numbers of 0 and 0.05, the TL_{max} corresponding to the first resonant frequency decreases and for others increase. In M_a =0.1 the TL_{max} corresponding to the first and the second resonant frequencies decreases and for the third resonant frequency increases.

Another point in Figs 10 and 15 is the pattern of resonant frequency generation in different serial HR array configurations. In other words, with the addition of each new HR array, the new resonant frequency is generated. Fig. 16 displays the fitting curve for resonant frequency from numerical results for different serial HR array configurations and various Mach numbers. According to this figure, the approximate value of the resonant frequency is equal to the product of 89 (resonant frequency for single HR in M_a =0) in the number of serial HR arrays. This conclusion is limited to the simulation results of this article.

In Fig. 10 the TL index is shown to investigate the acoustic transmission performance in the
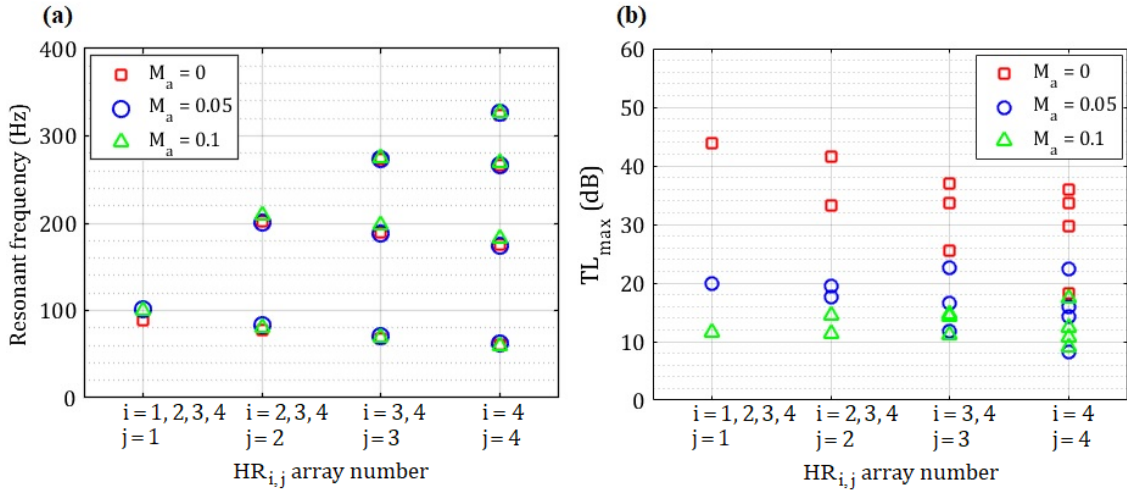
Fig. 15 (a) Resonant frequency (b) maximum transmission loss for different serial HR arrays
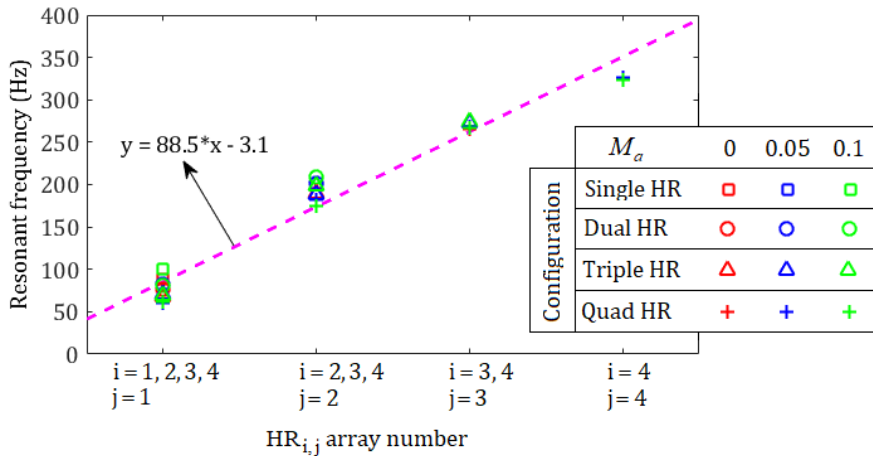
Fig. 16 The fitting curve for resonant frequency

frequency domain. However, it is not sufficient to analyze the attenuation characteristics quantitatively. The concept of energy storage capacity, based on the TL index, represents a suitable parameter to investigate the ability and acoustic attenuation performance of different configurations such as a conventional HR or an array (Cai and Mac 2018). The energy storage capacity is calculated according to the following equation,

$$C_{TL} = \int TL df = \sum_{i=0}^{f} \frac{TL_i + TL_{i+1}}{2} (f_{i+1} - f_i) \tag{12}$$

where C_{TL} is the energy storage capacity, f is the frequency and i is the counter, Fig. 17 exhibits C_{TL} against the number of serial HR arrays. It can be observed that the number of serial HR arrays has little effect on C_{TL}. In other words, the area under the TL-f curve in Fig. 10, which is equivalent which is equivalent to the acoustic attenuation performance, has not significantly
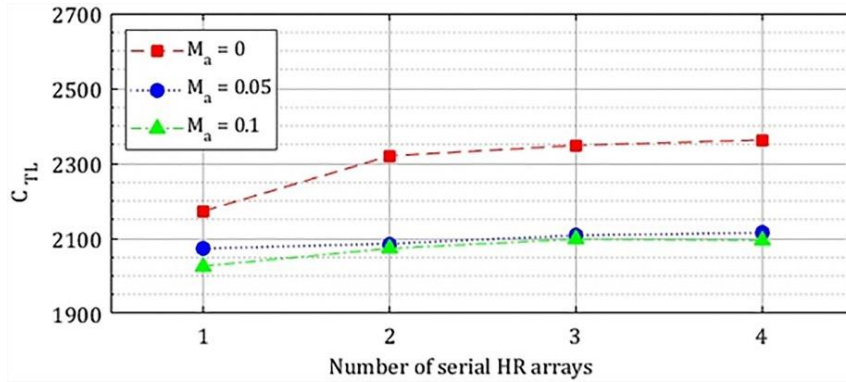
Fig. 17 Energy storage capacity for serial HRs array configurations
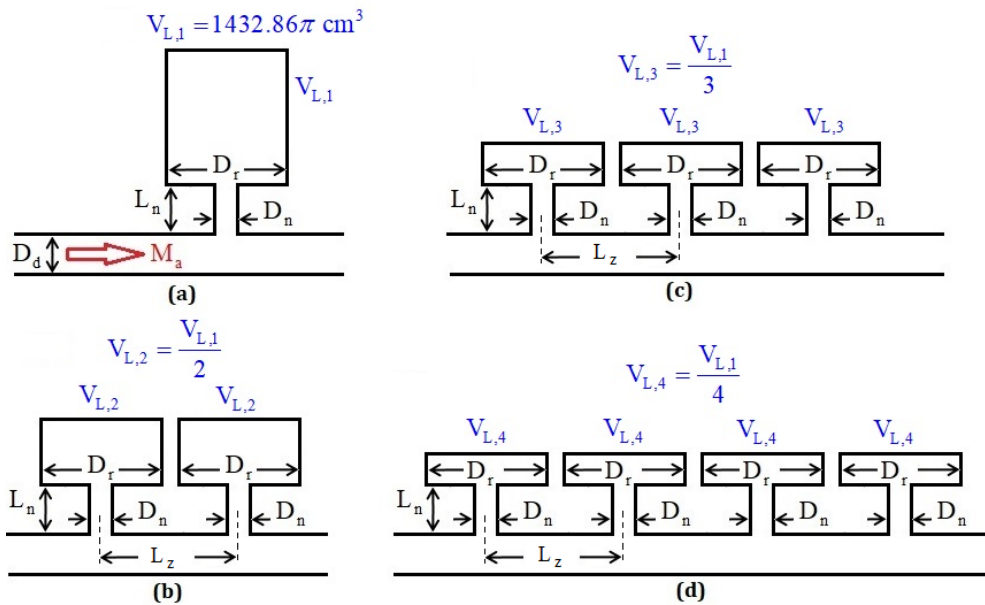
Fig. 18 Schematic of lined HR array with (a) one (b) two (c) three and (d) four resonator cavity

changed with increasing the number of serial HR arrays. Of course, the presence or absence of grazing flow affects the C_{TL}, so by setting up a grazing flow in the duct, there is about an 11% reduction in C_{TL}.

3.2 A lined Helmholtz resonator array

A conventional HR (single HR) has a transmission loss (TL) peak at its resonant frequency. Combining several HRs in a line is a possible way to increase TL peak and improve noise attenuation. In this section, the acoustic performance of one, two, three, and four-lined HR arrays will be evaluated in the presence of grazing flow. Fig. 18 presents a schematic of the lined HR array. The resonator cavity volume for all configurations is equal to each resonator cavity volume for all configurations is equal to each other, i.e $V_{L,1}=2V_{L,2}=3V_{L,3}=4V_{L,4}=1432.86\pi$ cm^3. The

Table 3 Geometry dimensions and flow conditions of the Lined HR array

Parameter	Value	Parameter	Value
L_u (cm)	70	$V_{L,1}$ (cm^3)	1432.86π
L_d (cm)	120	$V_{L,2}$ (cm^3)	716.43π
L_n (cm)	8.05	$V_{L,3}$ (cm^3)	477.62π
L_z (cm)	20	$V_{L,4}$ (cm^3)	358.22π
D_d (cm)	4.859	M_a	0 – 0.10
D_n (cm)	4.044	f (Hz)	5 - 500

Table 3 Geometry dimensions and flow conditions of the Lined HR array

Configuration	Theoretical Resonance Frequency (Eq. 14)	Predicted Resonance frequency (Hz)
RF$_{four\_lined\_HR}$	2 ×RF $_{One\ HR}$	2*90=180
RF$_{three\_lined\_HR}$	$\sqrt{3}$ ×RF $_{One\ HR}$	$\sqrt{3} * 90 = 155$
RF$_{two\_lined\_HR}$	$\sqrt{2}$ ×RF $_{One\ HR}$	$\sqrt{2} * 90 = 127$

geometry dimensions of Helmholtz resonator configurations and the other required parameters are presented in Table 3. The simulations are performed for various HR configurations according to Fig. 18 in grazing flow Mach numbers of 0, 0.05, and 0.10.

Fig. 19 demonstrates the TL versus frequency for lined HR array configurations including conventional (one), two, three, and four HR arrays (Fig. 17) in three Mach numbers of 0, 0.05, and 0.1. The resonant frequency of a conventional HR (Fig. 17a) can be theatrically determined by using the following equation (Zhao and morgans 2009)

$$RF_{theo} = \frac{1}{2\pi} \sqrt{\frac{c^2 S}{V L_{eff}}} \tag{13}$$

where c is the speed of sound, S is the cross section area of the resonator neck, V is the volume of the resonator and L_{eff} is the effective length of the resonator neck. With the parameters listed in Table 3, the theoretical predictions of the resonant frequency is 102 Hz and it is about 90 Hz in numerical simulation (Fig. 19). According to Fig. 19, TL$_{max}$ frequency increases as the number of lined resonators increases. This frequency shift is due to the decrease in the volume of each resonator as the number of lined resonators increases. The relationship between the resonance frequency of a Helmholtz resonator and the cavity volume is given by the Helmholtz formula, Eq. 13.

$$RF_{theo} \propto \frac{1}{\sqrt{V}} \tag{14}$$

We know that in lined configuration: $V_{L,1}=2V_{L,2}=3V_{L,3}=4V_{L,4}$. The predicted value of RF are listed in table 4. According to table 4, Predicted Resonance frequency is in good agreement with numerical simulation (Fig. 19).

Fig. 20 illustrates the quantitative value of the resonant frequency and TL$_{max}$ for the different lined HR array configurations on the various M_a. As can be observed in these figures, with increasing the number of lined HR arrays, the resonant frequency and TL$_{max}$ increase so that, with
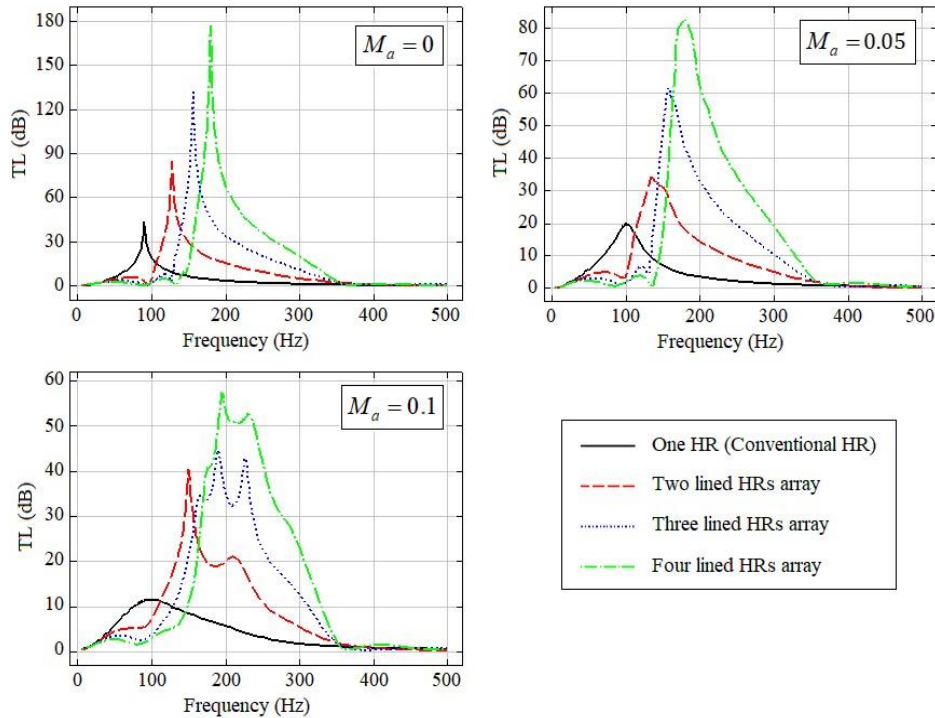
Fig. 19 Transmission loss versus frequency for the different lined array configurations in various M_a
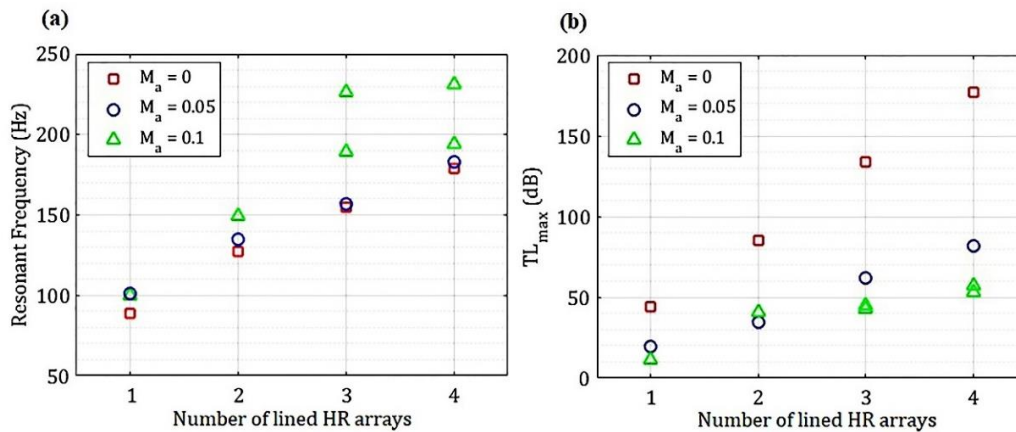
Fig. 20(a) Resonant frequency (b) maximum transmission loss for different lined HRs array

changing configuration from one array to four arrays 304%, 297%, and 394% increase in TL_{max} is seen for Mach numbers of 0.0, 0.05 and 0.1 respectively. Furthermore, for resonant frequency, the increase percentage is 101%, 66%, and 94% for Mach numbers of 0.0, 0.05, and 0.1, respectively. Figs. 21 to 23 show the flow velocity, total acoustic pressure and sound pressure level for the different lined array configurations in M_a =0.05 respectively. As can be seen this figures with changing configuration, flow and acoustics properties change.
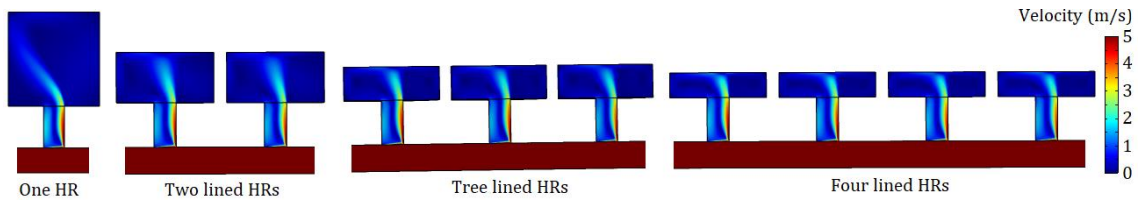
Fig. 21 Velocity contour (Steady State) for the different lined HRs array configurations in M_a=0.05
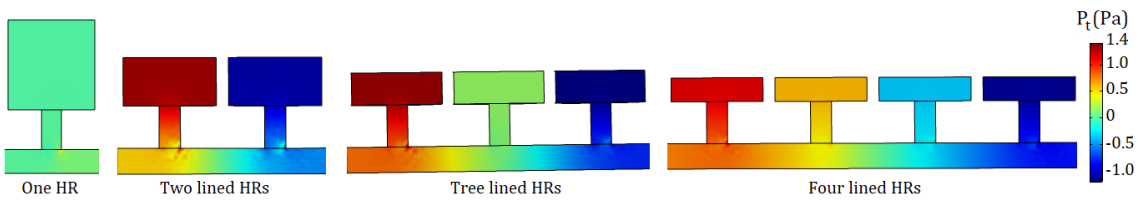
Fig. 22 Total acoustic pressure (Frequency-Domain at 100 Hz) for the different lined HRs array configurations in M_a=0.05
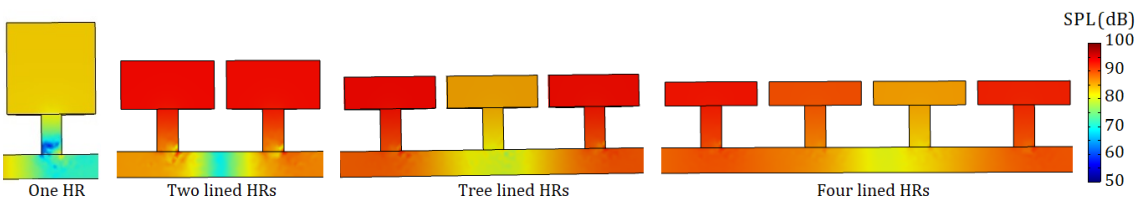
Fig. 23 Sound pressure level (Frequency-Domain at 100 Hz) for the different lined HRs array configurations in M_a=0.05
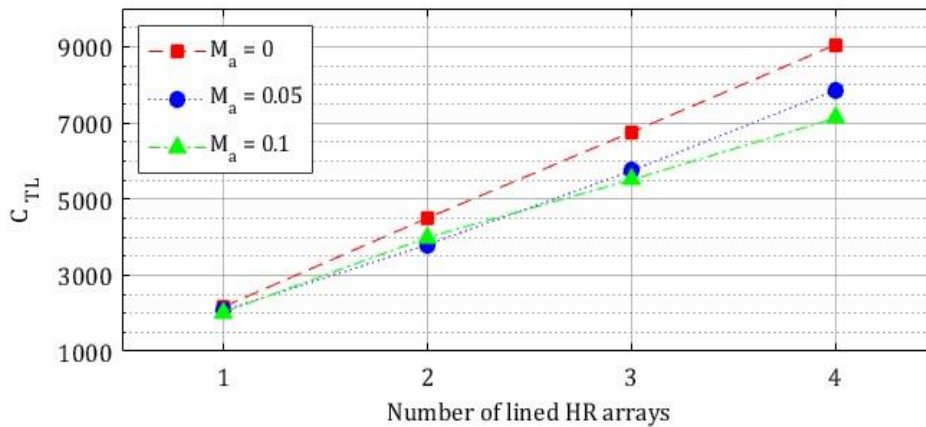
Fig. 24 Energy storage capacity for Lined HR array configurations

Fig. 15 demonstrates C_{TL} against the number of lined HR arrays. As can be seen, with increasing the number of lined HR arrays, the acoustic attenuation performance increases so that, with changing configuration from conventional HR (Fig. 18a) to a four-lined HR array (Fig. 18d) with the same total resonator cavity volume, 316%, 278% and 251% increase in C_{TL} is seen for Mach numbers of zero, 0.05 and 0.1 respectively.

$$V_c = 4V_l = 1432.86\pi \ cm^3$$
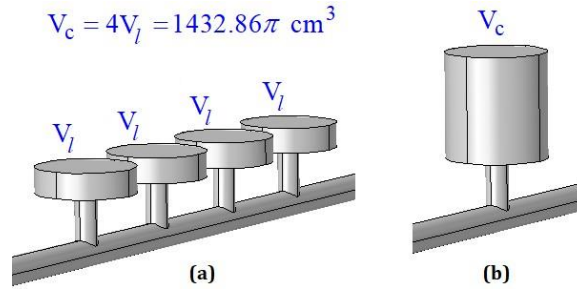
Fig. 25 A schematic of (a) four-lined HR array (b) conventional HR
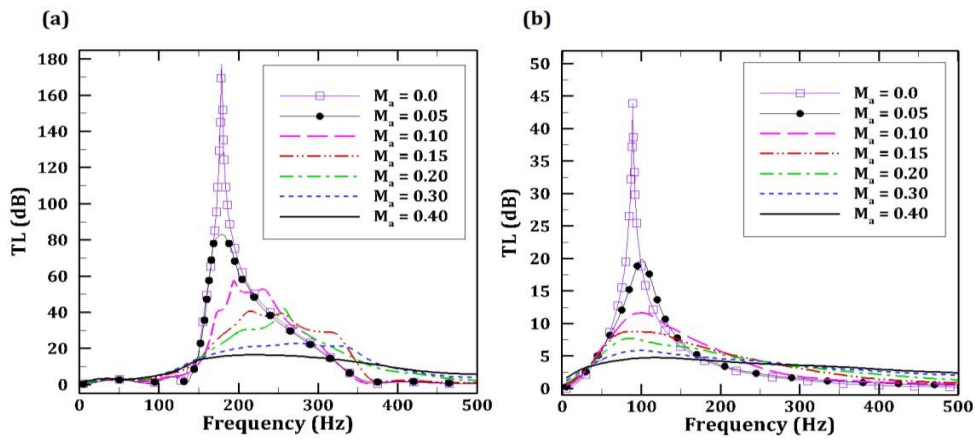
Fig. 26 Transmission loss against frequency, (a) four-lined HR array, and (b) conventional HR con figurations

3.3 The grazing flow Mach number effect

In this section, we investigate the effect of the grazing flow Mach number, *Ma*, on the four-lined HR array configuration and compare it to the conventional HR configuration. Fig. 25 shows a schematic of the configurations. The sum of resonators cavity volume for a four-lined HR array is equal to conventional HR, i.e. $V_c=4V_l=1432.86\pi \ cm^3$. The simulations are performed in various Mach numbers of 0.0, 0.05, 0.10, 0.15, 0.20, 0.30 and 0.40. The dimensions of conventional HR and four-lined HR array configurations are in accordance with Fig. 18, (a) and (d), respectively.

Fig. 26 depicts the TL against frequency in various Mach numbers for two configurations of conventional HR and a four-lined HR array. It can be seen in this figure, that the TL versus frequency has an increasing-decreasing trend and has a peak (maximum transmission loss) in resonant frequency. Fig. 27, corresponding to Fig. 26, shows the maximum transmission loss, TL_{max}, for various M_a and two configurations. In addition, Fig. 28 demonstrates Energy storage capacity, C_{TL}, as the quantitative attenuation characteristic, against M_a for two configurations. As can be seen in the figures, with increasing Mach number TL_{max} and C_{TL} decrease for both configurations. In addition, it is observed that the four-lined HR array configuration has a better acoustic performance than the conventional HR configuration. In Table 5 the increment percentage in TL_{max} and C_{TL} (δ_i) has been presented with changing configuration from the conventional HR to the four-lined HR array. δ_i is calculated using Eq. 14,
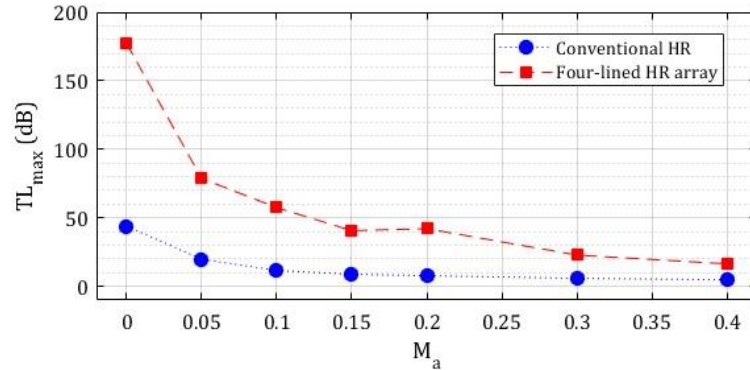
Fig. 27 Maximum transmission loss versus Mach number
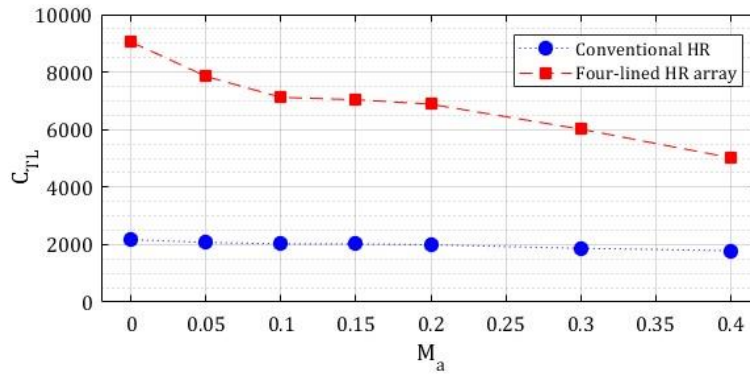
Fig. 28 Energy storage capacity versus Mach number

Table 5 Acoustic performance comparison of two configurations

Mach number	Four-Lined HR array		Conventional HR		$\delta_{TL_{max}}$ (%)	$\delta_{C_{TL}}$ (%)
	TL_{max} (dB)	C_{TL} (dB.Hz)	TL_{max} (dB)	C_{TL} (dB.Hz)		
0.0	177.25	9045.60	43.86	2173.03	304.13	316.26
0.05	83.02	7848.94	19.83	2073.10	297.17	278.62
0.10	57.45	7120.42	11.62	2026.31	394.40	251.39
0.15	40.65	7037.90	8.85	2022.12	364.57	248.04
0.20	42.05	6881.49	7.71	1992.61	445.39	245.35
0.30	22.80	6015.08	5.85	1871.16	289.74	221.46
0.40	16.40	5022.12	4.75	1788.24	245.26	180.84

$$\delta_i = \frac{\lfloor i \rfloor_{\text{ four-lined HR array}} - \lfloor i \rfloor_{\text{ conventional HR}}}{\lfloor i \rfloor_{\text{ conventional HR}}} \times 100 \tag{14}$$

where i represents TL_{max} and C_{TL}. As can be seen in table 5, with changing configuration from the conventional HR to four-lined HR array, 304% increase in TL_{max} and 316% increase in C_{TL} for M_a

= 0 occur. As the Mach number increases, this increment percentage decreases so that, for M_a =0.4 it reaches 245% and 180% for TL_{max} and C_{TL}, respectively.

Another important issue in Fig. 26 is that the conventional HR practically losts its performance as a tonal noise absorber for $M_a > 0.1$. While the four-lined HR array configuration to $M_a = 0.2$ acts as a tonal absorber.

4. Conclusions

In this paper, we investigated the effect of configuration type on the acoustic performance of HR in the presence of grazing flow. We considered two configurations: serial HR array and lined HR array, in association with turbofan acoustic liners. A serial HR array is formed by connecting several conventional HRs in series. A dual HR array, i.e., neck-cavity-neck-cavity, is the simplest serial HR array and is equivalent to a part of a DDOF acoustic liner. A lined HR array is formed by combining several conventional HRs in a line and is equivalent to a part of an SDOF acoustic liner. We used a 3D numerical approach, and COMSOL Multiphysics software was utilized for this purpose. The numerical approach was validated by comparing it with experimental data. This comparison confirmed the accuracy and precision of the numerical approach.

In the serial HR array, the simulations were performed for single, dual, triple, and quad HR arrays in the Mach numbers of 0.0, 0.05, and 0.10. Here, the resonator cavity volume for all configurations is equal to each other. The simulation results showed that for any serial HR array configuration, the number of resonant frequencies is equal to the number of serial HR arrays. Also, the acoustic attenuation performance, C_{TL} (the area under the TL-f curve), has not significantly changed with increasing the number of serial HR arrays. Moreover, the resonant frequencies decrease with increasing the number of HR arrays. In contrast, the TL$_{max}$ has a different treatment so that with increasing the number of HR arrays in the Mach numbers of 0 and 0.05, the TL$_{max}$ corresponding to the first resonant frequency decreases and for others increase. In M_a = 0.1 the TL$_{max}$ corresponding to the first and the second resonant frequencies decreases and for the third resonant frequency increases.

In the lined HR array, the simulations were performed for one (conventional HR), two, three, and four-lined HR arrays in the Mach numbers of 0.0, 0.05, and 0.10. The total resonator cavity volume for all lined HR array configurations is equal to each other. The results demonstrated that increasing the number of lined HR arrays, the resonant frequency, TL_{max} and C_{TL} increase so that, with changing configuration from the conventional HR to the four-lined array 304%, 297% and 394% increase in TL_{max} is seen for for Mach number of 0.0, 0.05 and 0.1, respectively. For the resonant frequency, the percentage increase is 101%, 66% and 94% for Mach numbers of 0.0, 0.05 and 0.1, respectively. Furthermore, 316%, 278 and 251% increase in C_{TL} is seen for Mach numbers of 0.0, 0.05 and 0.1, respectively.

The grazing flow Mach number's effect was investigated in the four-lined HR array configuration and compared with the conventional HR. The sum of resonators' cavity volume for the four-lined HR array is equal to conventional HR. The simulations were performed in various Mach numbers of 0.0, 0.05, 0.10, 0.15, 0.20, 0.30 and 0.40. The simulation results depict that with increasing Mach number, TL$_{max}$ and C_{TL} decrease. In addition, it was observed that the four-lined HR array configuration has a better acoustic performance than the conventional HR configuration. so that, with changing configuration from the conventional HR to the four-lined HR array, 304% increase in TL_{max} and 316% increase in C_{TL} occur for M_a =0. As the Mach number increases, this

increment percentage decreases so that, number increases, this increment percentage decreases so that, for Ma=0.4, it reaches 245% and 180% for $TLmax$ and CTL, respectively.

The results of this investigation showed that the serial HR array configuration can be helpful in the design of turbofan acoustic liners if the purpose is to reduce noise in several frequencies. The number of resonant frequencies is equal to the number of serial HR arrays. However, if the purpose is to increase the performance of acoustic liners in the resonant frequency, increasing the array number in the lined configuration at flow direction leads to increasing the maximum transmission loss (TL_{max}). The TL_{max} value is directly related to the number of lined HR arrays.

References

Bertolucci, B.L. (2012), "An experimental investigation of the grazing flow impedance duct at the University of Florida for acoustic liner applications", Ph.D. Dissertation, University of Florida.

Bi, R., Liu, Z.S., Li, K. M., Chen, J. and Wang, Y. (2012), "Helmholtz resonator with extended neck and absorbing material", *Appl. Mech. Mater.*, **141**, 308-312.
https://doi.org/10.4028/www.scientific.net/AMM.141.308.

Cai, C. and Mak, C.M. (2018), "Acoustic performance of different Helmholtz resonator array configurations", *Appl. Acoust.*, **130**, 204-209. https://doi.org/10.1016/j.apacoust.2017.09.026.

Chanaud, R.C. (1994), "Effects of geometry on the resonance frequency of Helmholtz resonators", *J. Sound Vib.*, **178**(3), 337-348. https://doi.org/10.1006/jsvi.1994.1490.

COMSOL Multiphysics software (2020), Acoustics Module Users Guide.

Dastourani, H. and Bahman-Jahromi, I. (2021), "Evaluation of aeroacoustic performance of a helmholtz resonator system with different resonator cavity shapes in the presence of a grazing flow", *J. Aerosp. Eng.*, **34**(5), 04021061. https://doi.org/10.1061/(ASCE)AS.1943-5525.0001309.

Dickey, N.S. and Selamet, A. (1996), "Helmholtz resonators: one-dimensional limit for small cavity length-to diameter ratios", *J. Sound Vib.*, **195**(3), 512-517. https://doi.org/10.1006/jsvi.1996.0440.

Guan, D., Zhao, D. and Ren, Z. (2020), "Aeroacoustic attenuation performance of a Helmholtz resonator with a rigid baffle implemented in the presence of a grazing flow", *Int. J. Aerosp. Eng.*, 1-16.
https://doi.org/10.1155/2020/1916239.

Igali, D., Wei, D., Zhang, D. and Perveen, A. (2020), "A comparative analysis of sheeting die geometries using numerical simulations", *Adv. Comput. Des.*, **5**(2), 111-125.
https://doi.org/10.12989/acd.2020.5.2.111.

Ingard, U. (1953), "On the theory and design of acoustic resonators", *J. Acoust. Soc. Am.*, **25**(6), 1037-1061.
https://doi.org/10.1121/1.1907235.

Jing, X.D., Wang, Y.J., Du, L., Qiu, X.H. and Sun X.F. (2023), "Impedance eduction experiments covering higher frequencies based on the multimodal straightforward method", *Appl. Acoust.*, **206**, 109327.
https://doi.org/10.1016/j.apacoust.2023.109327

Langfeldt, F., Hoppen, H. and Gleine, W. (2020), "Broadband low-frequency sound transmission loss improvement of double walls with Helmholtz resonators", *J. Sound Vib.*, **476**, 115309.
https://doi.org/10.1016/j.jsv.2020.115309.

Li, Y., Wang, X. and Zhang, D. (2013), "Control strategies for aircraft airframe noise reduction", *Chinese J. Aeronaut.*, **26**(2), 249-260. https://doi.org/10.1016/j.cja.2013.02.001.

Lu, Z., Pan, W. and Guan, Y. (2019), "Numerical studies of transmission loss performances of asymmetric Helmholtz resonators in the presence of a grazing flow", *J. Low Freq. Noise V. A.*, **38**(2), 244-254.
https://doi.org/10.1177/1461348418817914.

Ma, X. and Su, Z. (2020), "Development of acoustic liner in aero engine: A review", *Sci. China Technol. Sci.*, **63**(12), 1-14. https://doi.org/10.1007/s11431-019-1501-3.

Mahesh, K., Kumar Ranjith, S. and Mini, R.S. (2021), "Inverse design of a Helmholtz resonator based lowfrequency acoustic absorber using deep neural network", *J. Appl. Phys.*, **129**(17), 174901.

https://doi.org/10.1063/5.0046582.

Mahesh, K. and Mini, R.S. (2021), "Investigation on the acoustic performance of multiple Helmholtz resonator configurations", *Acoust. Australia*, **49**(2),355-69. https://doi.org/10.1007/s40857-021-00231-8.

Meissner, M. (2002), "Excitation of Helmholtz resonator by grazing air flow", *J. Sound Vib.*, **256**(2), 382-388. https://doi.org/10.1006/jsvi.2001.4219.

Rode, B.R. and Khare, R. (2021), "A review on development in design of multistage centrifugal pump", *Adv. Comput. Des.*, **6**(1), 43-53. https://doi.org/10.12989/acd.2021.6.1.043.

Selamet, A. and Ji, Z.L. (2000), "Circular asymmetric Helmholtz resonators", *J. Acoust. Soc. Am.*, **107**(5), 2360-2369. https://doi.org/10.1121/1.428622.

Selamet, A. and Lee, I. (2003), "Helmholtz resonator with extended neck", *J. Acoust. Soc. Am.*, **113**(4), 1975-1985. https://doi.org/10.1121/1.1558379.

Selamet, A., Radavich, P.M., Dickey, N.S. and Novak, J.M. (1997), "Circular concentric Helmholtz resonators", *J. Acoust. Soc. Am.*, **101**(1), 41-51. https://doi.org/10.1121/1.417986.

Selamet, E., Selamet, A., Iqbal, A. and Kim, H. (2011), "Effect of flow on Helmholtz resonator acoustics: a three-dimensional computational study vs. experiments", *SAE Technical Paper.*, No. 2011-01-1521. https://doi.org/10.4271/2011-01-1521.

Sugimoto, R., Murray, P. and Astley, R.J. (2012), "Folded cavity liners for turbofan engine intakes", *Proceedings of the 18th AIAA/CEAS Aeroacoustics Conference*, 2291.

Wu, G., Lu, Z., Xu, X., Pan, W., Wu, W., Li, J. and Ci, J. (2019), "Numerical investigation of aeroacoustics damping performance of a Helmholtz resonator: Effects of geometry, grazing and bias flow", *Aerosp. Sci. Technol.*, **86**, 191-203. https://doi.org/10.1016/j.ast.2019.01.007.

Qiu, X., Du, L., Jing, X. and Sun, X. (2019), "The Cremer concept for annular ducts for optimum sound attenuation", *J. Sound Vib.*, **438**, 383-401.

Qiu, X., Xin, B., Wu, L., Meng, Y., Jing, X. (2018), "Investigation of straightforward impedance education method on single-degree-of-freedom acoustic liners", *Chinese J. Aeronaut.*, **31**(12), 2221-2233. https://doi.org/10.1016/j.cja.2018.08.014.

Zhang, Z., Yu, D., Liu, J., Hu, B. and Wen, J. (2021), "Transmission and bandgap characteristics of a duct mounted with multiple hybrid Helmholtz resonators", *Appl. Acoust.*, **183**, 108266. https://doi.org/10.1016/j.apacoust.2021.108266.

Zhang, Z., Zhao, D., Han, N., Wang, S. and Li, J. (2015), "Control of combustion instability with a tunable Helmholtz resonator", *Aerosp. Sci. Technol.*, **41**, 55-62. https://doi.org/10.1016/j.ast.2014.12.011.

Zhao, D. (2011), "A real-time plane-wave decomposition algorithm for characterizing perforated liners damping at multiple mode frequencies", *J. Acoust. Soc. Am.*, **129**(3), 1184-1192. https://doi.org/10.1121/1.3533724

Zhao, D. (2012), "Transmission loss analysis of a parallel-coupled Helmholtz resonator network", *AIAA J.*, **50**(6), 1339-1346.

Zhao, D., Ji, C. and Yin, M. (2022), "Experimental investigation of geometric shape effect of coupled Helmholtz resonators on aeroacoustics damping performances in presence of low grazing flow", *Aerosp. Sci. Technol.*, **128**, 107799. https://doi.org/10.1016/j.ast.2022.107799

Zhao, D. and Morgans, A.S. (2009), "Tuned passive control of combustion instabilities using multiple Helmholtz resonators", *J. Sound Vib.*, **320**(4-5), 744-757.

Zhao, X., Cai, L., Yu, D., Lu, Z. and Wen, J. (2017), "A low frequency acoustic insulator by using the acoustic metasurface to a Helmholtz resonator", *AIP Adv.*, **7**(6), 065211. https://doi.org/10.1063/1.4989819.

Žilienė, D., Stankūnas, J. (2002), "Analysis of the influence of aircraft noise limitations following requirements of European Union on the sector of Lithuania air transport services", *Aviation*, **6**, 34-40.

CC